Article

Rhizosphere Bacterium *Rhodococcus* sp. P1Y Metabolizes Abscisic Acid to Form Dehydrovomifoliol

Oleg S. Yuzikhin [1,2], Natalia E. Gogoleva [3,4], Alexander I. Shaposhnikov [1], Tatyana A. Konnova [5], Elena V. Osipova [3], Darya S. Syrova [1], Elena A. Ermakova [3], Valerii P. Shevchenko [6], Igor Yu. Nagaev [6], Konstantin V. Shevchenko [6], Nikolay F. Myasoedov [6], Vera I. Safronova [1], Alexey L. Shavarda [7], Anton A. Nizhnikov [1,7], Andrey A. Belimov [1] and Yuri V. Gogolev [3,4,*]

1   All-Russia Research Institute for Agricultural Microbiology, Podbelskogo sh. 3, Pushkin, 196608 Saint-Petersburg, Russia; yuzikhin@gmail.com (O.S.Y.); ai-shaposhnikov@mail.ru (A.I.S.); syr_daria@ro.ru (D.S.S.); v.safronova@rambler.ru (V.I.S.); a.nizhnikov@arriam.ru (A.A.N.); belimov@rambler.ru (A.A.B.)
2   All-Russian Research Institute of Plant Protection, Podbelskogo sh. 3, Pushkin, 196608 Saint-Petersburg, Russia
3   Kazan Institute of Biochemistry and Biophysics, Federal Research Center "Kazan Scientific Center of the RAS", Lobachevsky Street, 2/31, 420111 Kazan, Tatarstan Republic, Russia; negogoleva@gmail.com (N.E.G.); eva-0@mail.ru (E.V.O.); ermakova@kibb.knc.ru (E.A.E.)
4   Kazan Federal University Institute of Fundamental Medicine and Biology, K.Marx, 76, 420012 Kazan, Russia
5   Laboratory of Plant Infectious Diseases, FRC Kazan Scientific Center of RAS, 420111 Kazan, Tatarstan Republic, Russia; tatiana.a.konnova@gmail.com
6   Institute of Molecular Genetics, Russian Academy of Sciences, Akademika Kurchatova Square, 2, 123182 Moscow, Russia; ATCarma@mail.ru (V.P.S.); nagaev@img.ras.ru (I.Y.N.); ATRegister@mail.ru (K.V.S.); nfm@img.ras.ru (N.F.M.)
7   Department of Genetics and Biotechnology, Saint-Petersburg State University, University Embankment, 199034 Saint-Petersburg, Russia; shavarda@binran.ru
*   Correspondence: gogolev.yuri@gmail.com; Tel.: +7-917-916-8381

Abstract: The phytohormone abscisic acid (ABA) plays an important role in plant growth and in response to abiotic stress factors. At the same time, its accumulation in soil can negatively affect seed germination, inhibit root growth and increase plant sensitivity to pathogens. ABA is an inert compound resistant to spontaneous hydrolysis and its biological transformation is scarcely understood. Recently, the strain *Rhodococcus* sp. P1Y was described as a rhizosphere bacterium assimilating ABA as a sole carbon source in batch culture and affecting ABA concentrations in plant roots. In this work, the intermediate product of ABA decomposition by this bacterium was isolated and purified by preparative HPLC techniques. Proof that this compound belongs to ABA derivatives was carried out by measuring the molar radioactivity of the conversion products of this phytohormone labeled with tritium. The chemical structure of this compound was determined by instrumental techniques including high-resolution mass spectrometry, NMR spectrometry, FTIR and UV spectroscopies. As a result, the metabolite was identified as (4*RS*)-4-hydroxy-3,5,5-trimethyl-4-[(*E*)-3-oxobut-1-enyl]cyclohex-2-en-1-one (dehydrovomifoliol). Based on the data obtained, it was concluded that the pathway of bacterial degradation and assimilation of ABA begins with a gradual shortening of the acyl part of the molecule.

Keywords: abscisic acid; microbial metabolite; dehydrovomifoliol; NMR spectrometry; phytohormones; rhizosphere; *Rhodococcus*

1. Introduction

Abscisic acid (ABA) controls numerous aspects of the plant life cycle, including seed dormancy, germination and adaptive responses to environmental stresses [1]. The content of ABA in plant tissues is determined by the balance of its biosynthesis and catabolism. In plant catabolism, ABA does not undergo deep degradation, but is converted

to inactive forms by oxidation or conjugation reactions [2,3]. The oxidation is the main pathway of ABA inactivation in plants. The key reaction of this pathway is hydroxylation at C-8′ to produce 8′-hydroxy ABA. It has been shown that in *Arabidopsis thaliana,* this reaction is catalyzed by the CYP707A2 monooxygenase [4]. 8′-hydroxy ABA spontaneously isomerizes to phaseic acid (PA) [5]. Significant amounts of ABA and, apparently, the products of its catabolism are constantly introduced into soil via the decomposition of abscised shoot tissues and root turnover. It has been shown that ABA transporters located in root epidermal cells can efflux ABA and its concentration in the soil solution can gradually increase during the growing season [6].

Higher plants are not monopolists in the production of ABA. ABA has been found at low concentrations in a wide range of tested organisms such as bacteria, cyanobacteria, algae, bryophytes, fungi and lichens [2,7]. Although often referred to as a phytohormone, ABA is an effective regulator of stress responses and pathogen biology in plants, parasitic protozoans, sponges, hydroids, insects, and mammals [8]. As shown in *Apis mellifera*, in insects, ABA may be involved in wound healing, pesticide sensitivity, and cold resistance [9]. Studies in mammals have also demonstrated the capacity of mammalian cells to respond to exogenous ABA. Biological responses include wide-ranging effects on inflammation, cell proliferation and glucose tolerance [10]. Until recently it was well accepted that bacteria do not synthesize ABA. However, in 2007, ABA was found in isolated strains of endophytic bacteria in the roots of *Helianthus annuus* [11]. Then, the ability to synthesize ABA was found in several plant growth-promoting rhizobacteria (PGPR), including *Azospirillum lipoferum* [12], *Arthrobacter koreensis* [13], *Achromobacter xylosoxidans*, *Bacillus licheniformis*, *Bacillus pumilus* and *Brevibacterium halotolerans* [14]. Fungi produce relatively large amounts of ABA that could be released into the environment [15]. Although little is known about the role of ABA in the metabolism of fungi, fungal ABA may be of some importance for plants infected with ABA-producing phytopatogenic fungi, in mycorrhizal associations and lichens [7]. In particular, there is ample evidence that ABA production is a significant contributor to the virulence of fungal phytopathogens [16,17].

The accumulation of ABA in soil can have a variety of effects on the development, resistance, and fitness of plants. Particularly, ABA accumulation during water stress may play a role in maintaining plant water status and growth in drying soil [18,19]. On the other hand, exogenous ABA can inhibit or promote root growth of well-watered plants depending on the phytohormone concentration [20–22]. Exogenous ABA decreased the elongation rate in maize coleoptiles [23]. The addition of ABA to mature non-dormant seeds has been shown to inhibit their germination. This effect of ABA might be related to its natural function as an endogenous inhibitor of precocious germination during seed formation [24]. The application of exogenous ABA or the inhibition of ABA biosynthesis revealed that increased ABA levels correlated with an increased susceptibility of plants to fungal [25–27] and bacterial pathogens [28].

The negative effects of ABA accumulation should probably be offset by the processes of its conversion. Since it is assumed that plants can contribute to, but do not regulate, the ABA concentration in soil, the plant associated microorganisms can claim this role. This hypothesis is supported by evidence that PGPR influences the rhizosphere concentration of other phytohormones, such as auxins [17] and ethylene [29,30], through the utilization of hormones or their precursors as carbon and/or nitrogen sources. It was also shown that *Burkholderia phytofirmans* [31], *Pseudomonas putida* [32], and *Rhizobium* spp. [33] degraded indole-3-acetic acid. *Serratia proteamaculans* utilized the cytokinin N^6-benzyladenine [34], *Azospirillum* spp. transformed gibberellins [35] and several *Pseudomonas* spp. strains catabolized salicylic acid [36,37]. Recently, strains of *Achromobacter* sp., *Burkholderia* sp. and *Pseudomonas* sp. utilizing both indole-3-acetic and salicylic acids were identified [38]. However, information about the biochemistry of ABA biosynthesis and metabolism is very limited [7,8,39]. Nevertheless, there are results of preliminary studies that indicate the possible existence of more than one pathway of ABA catabolism in bacteria. In one study, it was shown that the introduction of radioactive ABA into non-sterile soil led to a rapid

decomposition of this compound to phaseic acid and dehydrophaseic acid [6]. Earlier, it was reported that a soil bacterium, phenotypically designated as *Corynebacterium* sp., growing on a medium with ABA (2 g L^{-1}) and yeast extract (1 g L^{-1}), accumulated a compound with spectral characteristics similar to those of dehydrovomifoliol [40]. Unfortunately, the exact chemical structure of this compound has not been established. No further information about this bacterium and its ecological role in plant-microbe interactions is available.

Recently, using a selective ABA-supplemented medium, two bacterial strains were isolated from the rhizosphere of rice (*Oryza sativa* L.) and assigned to *Rhodococcus* sp. P1Y and *Novosphingobium* sp. P6W [41]. Both strains could utilize ABA as a sole carbon source in batch culture and decrease ABA concentrations in tomato roots or leaves. Correlations between the effects of these bacteria on plant growth and ABA concentrations in planta suggested that ABA-metabolizing rhizobacteria may interact with plants via an ABA-dependent mechanism. Thus, the aforementioned study [42] highlighted the importance of studying these microorganisms and the metabolic pathways of microbial ABA degradation.

The present report aimed to isolate and identify the chemical structure of an intermediate metabolite of ABA degradation by *Rhodococcus* sp. P1Y by a selection of techniques including high-resolution mass spectrometry, NMR spectrometry, FTIR and UV spectroscopies. The pool of data obtained thereby unambiguously indicate that this metabolite is dehydrovomifoliol.

2. Materials and Methods

2.1. Labeling ABA with Tritium

ABA was purchased from Merck (Sigma-Aldrich, St. Louis, MO, USA). A method for tritium labeling of the cyclohexene part of the ABA molecule has been reported [42]. Briefly, the reaction tube was charged with PdO (60 mg), 5% Pd/BaSO$_4$ (15 mg) and anhydrous dioxane (0.3 mL). The tube was cooled with liquid nitrogen and evacuated down to 0.1 Pa, and tritium was injected up to 400 hPa pressure. Palladium oxide was reduced for 60–90 min at room temperature with stirring. The content of the tube was frozen in liquid nitrogen and evacuated down to 0.1 Pa to remove tritium. Dioxane and tritiated water were distilled into a tube containing 3 mg of ABA. The tube was filled with argon, diisopropylethylamine was added (4:1), and the reaction was conducted for 20 min at 220 °C. The reaction mixture was frozen in liquid nitrogen and volatile components were evaporated. The dry residue was dissolved in methanol. Labile tritium was removed by five times evaporation with methanol (3 mL). The residue was purified by HPLC on a Kromasil 100 C18 packed column (Eka Chemicals AB, Sweden, 8 × 150 mm size, 7 μm particle size) in a methanol:water:acetic acid solvent system (40:60:0.1) at a flow rate of 2 mL/min. The radiochemical purity of the product was analyzed on a Reprosil pur C18aq column (Dr. Maisch GmbH, Germany, 4 × 150 mm size, 5 μm particle size) using the following eluents: A, methanol:water:acetic acid (30:70:0.1); B, methanol; linear gradient from 0 to 50% of B in 15 min. The flow rate was 1 mL min^{-1}. The retention time was 5.3 min. The yield of ABA was 50% and the specific radioactivity was 30.5 Ci mmol^{-1}. The radiochemical purity of the final product was 98.5%.

2.2. Bacteria Cultivation

The bacterial culture cells were grown at 24 °C with shaking (200 rpm) in 100 mL of a mineral salt medium containing (g L^{-1}): 14-Na$_2$HPO$_4$·12H$_2$O, 3.0-KH$_2$PO$_4$, 1.0-NH$_4$Cl, 0.3-MgSO$_4$, 0.1-CaCl$_2$, pH = 6.5. The medium was supplemented with 25 mg of ABA (250 mg L^{-1}). When the cell culture absorbance reached 0.4 AU, an additional 25 of mg ABA and 50 μCi of labeled ABA was added. After 2 h of incubation, the bacterial suspension was centrifuged, and the supernatant was lyophilized.

Similar growth conditions and the medium were used to monitor the growth and utilization of putative low-molecular-weight products of the bacterial ABA metabolism, such as acetic, glycolic, glyoxylic and oxalic acids (Sigma-Aldrich). Bacterial growth was monitored daily by measuring the optical density of suspensions at 540 nm using a

SmartSpec Plus spectrophotometer (Bio-Rad Laboratories Inc., Hercules, CA, USA). ABA and fructose were used as positive controls.

2.3. HPLC-MS Analysis Conditions

The lyophilized supernatant was extracted three times with 50 mL portions of methanol using an ultrasonic bath. The combined extract was evaporated to dryness on a rotary evaporator at 40 °C. As a result, 34.1 mg of dry residue was obtained. The residue was dissolved in 10 mL of methanol and analyzed by HPLC-MS using a 6538 Q-TOF mass spectrometer (Agilent Technologies, Santa Clara, CA, USA) equipped with an ESI interface. A Waters BEH-C18 column (100 × 3.0 mm, 3.5 μm) was used. Chromatography was performed at ambient temperature with an injection volume of 5 μL. The flow rate was 0.15 mL/min. The mobile phases were water–acetonitrile 95:5 + 0.1% formic acid (A) and acetonitrile–water 90:10 + 0.1% formic acid (B). The gradient was as follows: 0–1 min 0% B, 1–13 min 0% → 90% B; 13–20 min, 90% B; and 20–25 min, 90% → 0% B. The Q-TOF/MS analysis was carried out in full-scan mode, and the mass range was m/z 100−2000 in the negative and positive modes, with a scan rate 2 spectra/sec. The operating parameters of the electrospray ionization sources were as follows: drying gas (N_2) flow rate, 7.0 L/min; drying gas temperature, 350 °C; nebulizer pressure, 30 psig; fragmentor voltage, 175 V; capillary, 3500 V; octapoleRFPeak, 750 V; and skimmer voltage, 65 V. All the acquisitions and analyses of data were controlled by MassHunter software (version B.05.00, Agilent Technologies, Santa-Clara, CA, USA). A calibrating solution (calibrant solution A, Agilent Technologies, Santa-Clara, CA, USA) containing internal reference masses at m/z 119.0363 and 966.0007 in negative and 121.050873 and 922.009798 in positive ion mode was used in conjunction with an automated calibration. Parallel UV detection was performed using an Agilent 1260 Series G1365D Multiple Wavelength Detector instrument.

2.4. Isolation of Metabolite I

The preparative chromatographic separation of the metabolites was performed on silica gel (Merck 60) using the MPLC system Buchi Sepacore and completed with the UV-Monitor C-630, two Pump Module C-605, Control Unit S-620, fractions collector C-660 (Buchi, Flawil, Switzerland). The solvents were (A) n-hexane, (B) EtOAc, and (C) MeOH. The methanol solution (obtained as described in Section 2.3) was loaded onto 5 mL of silica gel, blowing off methanol in a stream of nitrogen. The resulting material was introduced in hexane into a cartridge, which was connected in series with a Glass Column Buchi 15/230 (40.65 mL) filled with the same silica gel and preconditioned in a hexane flow (15 mL min^{-1} for 5 min). The separation conditions are shown in Table 1. Eluent flow rate was 15 mL min^{-1}. Fractions of 45 mL were collected and analyzed by liquid scintillation counting using a QuantaSmart Tri-Carb 2810TR instrument (PerkingElmer, Inc., Waltham, MA, USA). The purity and composition of the obtained fractions were estimated by the UPLC method using an Acquity H-class chromatograph with PDA detector. A Waters ACQUITY UPLC BEH C18 column (50 × 2.1 mm, 1.7 μm) was used for analysis. Chromatography was performed at 30 °C. The injection volume was 5 μL. The flow rate was 0.3 mL min^{-1}. The mobile phases were water with 0.1% formic acid (A) and acetonitrile with 0.1% formic acid (B). The gradient was as follows: 0–1 min 0% B, 1–13 min 0% → 90% B; 13–14.1 min 90% → 0% B. The detection wavelength was 265 nm. MPLC fractions 10 and 11, which showed high radioactivity and contained (as shown by UPLC analysis) one major component, were combined and evaporated to dryness at 40 °C using a vacuum rotary evaporator Heidolph Hei-VAP Precision (Heidolph Instruments GMBH and CO KG, Schwabach, Germany). The dry residue weight was 2.1 mg (6.2% yield).

The final purification of the compounds was carried out by preparative HPLC using a Waters 2545 HPLC completed with a 2489 UV/VIS detector, a Waters XBridge Prep C18 OBD column (250 × 19 mm, 5 μm) and a fraction collector III (Waters Corporation, Milford, MA, USA). Chromatography was performed at ambient temperature. Before the chromatographic separation, the dry residue obtained after MPLC separation was dissolved

in 5 mL of methanol. Injection volume was 1 mL. The flow rate was 5 mL min^{-1}. The mobile phases were water (A) and acetonitrile (B). The gradient was as follows: 0–1.5 min 0% B, 1.5–13.5 min 0% → 90% B; 13.5–15 min, 90% B; and 15–16 min, 90% → 0% B. The detection wavelength was 265 nm. Under the conditions of chromatography, the collection of ABA was carried out in the time interval of 8.2–9.0 min, and the target metabolite, in the interval of 7.2–7.7 min. The final solutions were pools of the corresponding fractions after five successive separations.

Table 1. Conditions for MPLC separation of metabolites and radioactivity of chromatographic fractions of the *Rhodococcus* sp. P1Y culture after incubation for 2 h in the presence of ^{3}H-labeled ABA.

No. of Fraction	Starting Solvents Ratio, Vol %	Final Solvents Ratio, Vol %	Radioactivity, cpm μL^{-1}
1	A 100	A-B 90:10	10.1 [1]
2	A-B 90:10	A-B 80:20	7.0
3	A-B 80:20	A-B 70:30	2.2
4	A-B 70:30	A-B 60:40	2.5
5	A-B 60:40	A-B 50:50	1.0
6	A-B 50:50	A-B 40:60	-
7	A-B 40:60	A-B 30:70	-
8	A-B 30:70	A-B 20:80	-
9	A-B 20:80	A-B 10:90	3.5
10	A-B 10:90	B 100	34.5
11	B 100	B-C 50:50	168.2
12	B-C 50:50	C 100	164.3
13	C 100	C 100	5.6

[1] The volume of each fraction was 45 mL.

After the evaporation of the solvent, 1.3 mg (yield 3.8%) of a chromatographically pure compound was obtained, which was analyzed by liquid scintillation counting and spectrometric analyses.

2.5. Spectrometric Analyses

A UV spectrum of metabolite I was recorded in the HPLC mode using a diode array detector. The spectrum was obtained in the solvent system water–acetonitrile (32%) with 0.1% formic acid, analytical flow cell with a volume of 500 nL and path length of 10 mm.

One- (^{1}H, WET1D) and two-dimensional (HSQC, HMBC, H2BC) nuclear magnetic resonance (NMR) spectra were recorded on a DirectDrive NMR System (Varian, Palo Aho, CA, USA) in CDCl$_3$ at 700 and/or 175.8 MHz. CDCl$_3$ was used as an internal standard.

For the FTIR spectroscopic measurements, 1 mg of the resulting substance was dissolved in 10 μL of methanol (99.9%, Acros Organics, Antwerp, Belgium), placed with a microsyringe as a thin film on clean flat CVD-ZnSe disks with the diameter of 10 mm and thickness of 2 mm (R'AIN Optics, Dzerzhinsk, Russia) and dried. Transmission FTIR spectroscopic measurements were performed on a Nicolet 6700 FTIR spectrometer equipped with a DTGS detector and a KBr beam splitter (Thermo Electron Corporation, Beverly, MA, USA). Spectra were collected with a total of 64 scans (resolution 4 cm^{-1}) against the CVD-ZnSe disc background and manipulated using the OMNIC software (version 8.2.0.387, Thermo Fisher Scientific, Waltham, MA, USA) supplied by the manufacturer of the spectrometer. The baseline was corrected using the "automatic baseline correct" function. The spectra were smoothed using the standard "automatic smooth" function of the software which uses the Savitsky–Golay algorithm (95-point moving second-degree polynomial). The FTIR spectroscopic measurements were repeated three times and were well reproducible.

2.6. Molecular Geometry Calculations

The geometry optimization of two enantiomers was performed by us using the GAUSSIAN program (version GAUSSIAN09, Gaussian, Inc., Wallingford, CT, USA) and the DFT method

at the b3lyp/6-311+G(d,p) level of theory.

2.7. Statistical Analysis

The statistical analysis of the data presented in Figure 7 was performed using the software STATISTICA version 10 (TIBCO Software Inc., Palo Alto, CA, USA).

3. Results

3.1. Identification and Isolation of Metabolite I

Strain *Rhodococcus* sp. P1Y grew well on the mineral medium containing ABA as a sole carbon source. Analysis of the culture fluid by the HPLC-MS revealed two major and several minor compounds, presumably microbial metabolites of this phytohormone (Figure 1). The present research focused on the purification and identification of the main compound, named metabolite I.
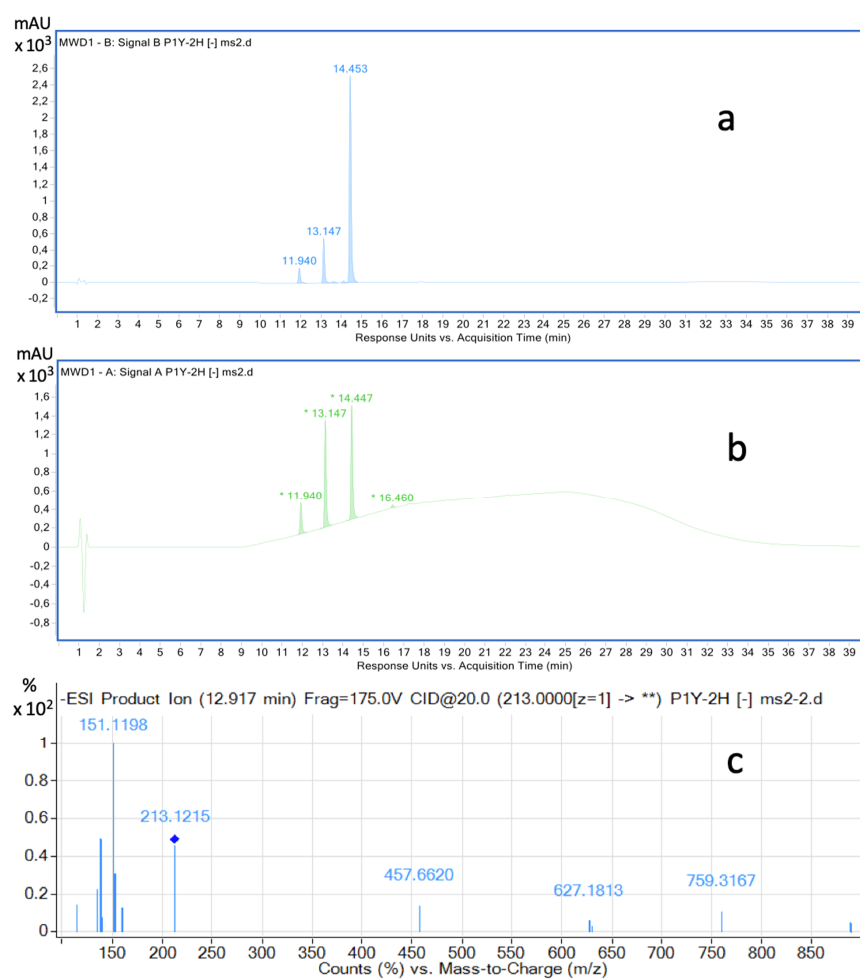
Figure 1. Chromatograms of the components of the *Rhodococcus* sp. P1Y culture liquid 2 h after adding the tritium labeled ABA. HPLC-MS, registration at two wavelengths: 254 nm (**a**) and 220 nm (**b**). Mass spectra of components: ESI–TOF MS, negative ion mode (**c**), E_{col} = 20 V m/z (relative intensity): compound 14.4, abscisic acid (ABA): 263.1291 ($C_{15}H_{19}O_4$, calcd. 263.1283) $[M-H]^-$ (100), 219.1392 ($C_{14}H_{19}O_2$, calcd. 219.1385) $[M-H-CO_2]^-$ (14); Compound 13.1 (metabolite I) (**c**): 213.1203 ($C_{11}H_{17}O_4$, calcd. 213.1127) $[M + 2H_2O- H-CH_3CHO]^-$ (45), 153.0951 ($C_9H_{13}O_2$, calcd. 153.0916) (31), 151.1198 ($C_{10}H_{15}O$, calcd. 151.1123) (100), 138.0747 ($C_8H_{10}O_2$, calcd. 138.0681) (49), 135.0874 ($C_9H_{11}O$, calcd. 135.0810) (22); compound 11.9: 212.1002 (^{13}C- Isotope ion, calcd. 212.1004) $[M-H + 1]^-$ (12), 211.0969 ($C_{11}H_{15}O_4$, calcd. 211.0970) $[M-H]^-$ (100), 167.1077 ($C_{10}H_{15}O_2$, calcd. 167.1072) $[M-H-CO_2]^-$ (41), 152.0834 ($C_9H_{12}O_2$, calcd. 152.0837) $[M-CH_3COOH]^-$ (8), 149.0972 ($C_{10}H_{13}O$, calcd. 149.0966) $[M-H-CO_2- H_2O]^-$ (9).

Experiments with a radioactive precursor confirmed that the detected compounds originate from ABA. When the microorganism was grown on 25 mg of labeled ABA (2384 cpm/µg, 284 mCi/mol), the radioactive substrate accumulated in two fractions of preparative chromatographic separation (Table 1). These fractions were re-separated in an acetonitrile–water system. After the evaporation of the solvent, chromatographic purification gave 1.3 mg of material (yield 3.8%) as a colorless oil. The purity of the isolated compound was established by the UPLC as described in the Materials and Methods (data not shown). The radioactivity of the obtained metabolite was 2562 cpm μg^{-1}, which is 263 mCi mol^{-1} (see below). This value corresponds well to the activity of ABA as a precursor.

3.2. Chromatography-Mass Spectrometric Measurements

ESI-TOF MS analysis in negative ionization mode has been performed for ABA and Compound I in HPLC-MS analysis of culture liquid components (Figure 1c). In this case, the molecular ion of metabolite I was not obtained. The main ions were ions with masses $M^- = 153.0916$ and 151.1123. The calculated structures of these ions are shown in Figure 2. These ions were obtained as a result of the detachment of the side chain of the ABA molecule, which indicates the intactness of the cyclohexene residue in metabolite I. The absence of a molecular ion in the spectra may be due to its instability and the absence of strong acid groups in the metabolite structure.
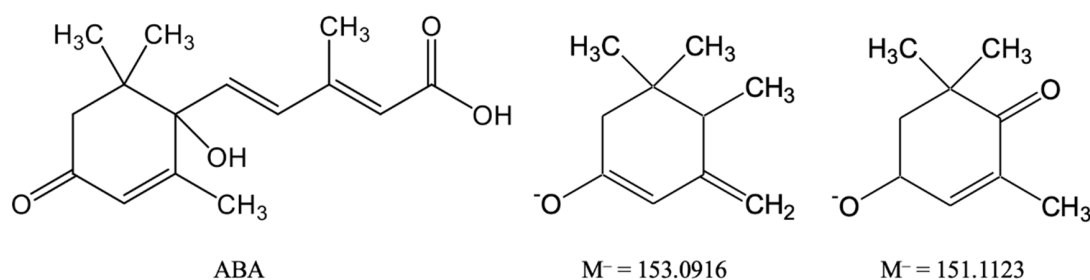

Figure 2. Calculated structures of the main ions obtained by ESI-TOF MS in negative ionization mode.

Mass spectra for the purified metabolite I were obtained in the positive electrospray ionization mode (Figure 3). The spectrum contained the molecular ion M^+ 223.1334, as well as the M^+ 205.1225 ion. The latter can be obtained as a result of the abstraction of a water molecule, which is typical for alcohols. However, the main ions were ions of deep fragmentation, probably associated with breaks in the cyclohexene part of the molecule.

3.3. NMR Spectroscopy

A detailed identification of the chemical structure of metabolite I was carried out using NMR methods, including one-dimensional (1H, WET1D) and two-dimensional (HSQC, HMBC, H2BC) experiments. The HSQC spectrum made it possible to establish the binding of carbon atoms with protons. Long-range carbon–proton interactions were obtained from the HMBC and H2BC spectra, which made it possible to establish the carbon skeleton of the molecule. A ^{13}C NMR spectrum of metabolite I was extracted from the corresponding 2D spectra. Below are the spectral characteristics and their corresponding interpretation. ^1H NMR: 6.83 (1H, d, J = 15.8 Hz, H-1′), 6.46 (1H, d, J = 15.7 Hz, H-2′), 5.96 (1H, dd, J = 1.2, 1.0 Hz, H-2), 2.50 (1H, dm, J = 17.2 Hz, H-6a), 2.34 (1H, dm, J = 17.1 Hz, H-6b), 2.30 (3H, s, H-4′), 1.88 (3H, d, J = 1.3 Hz H-5′), 1.82 (1H, d, J = 0.3 Hz, OH), 1.11 (3H, s, H-6′), 1.01 (3H, s, H-7′). ^{13}C NMR: 199.9 (C-3′, C=O), 199.6 (C-1, C=O), 162.7 (C-3, Cq), 147.3 (C-1′, HC=CH), 132.9 (C-2′, HC=CH), 130.3 (C-2, HC=C), 81.8 (C-4, C–OH), 52.1 (C-6, CH_2), 44.0 (C-5, Cq), 30.8 (C-4′, CH_3), 26.8 (C-7′, CH_3), 25.4 (C-6′, CH_3), 21.1 (C-5′, CH_3). UV (λ_{max}): 239.0 nm. More detailed information is given in the Supplementary File S1. The ABA spectra (Supplementary File S2) were obtained under the same conditions of the NMR experiment that were used for the studied metabolite I.
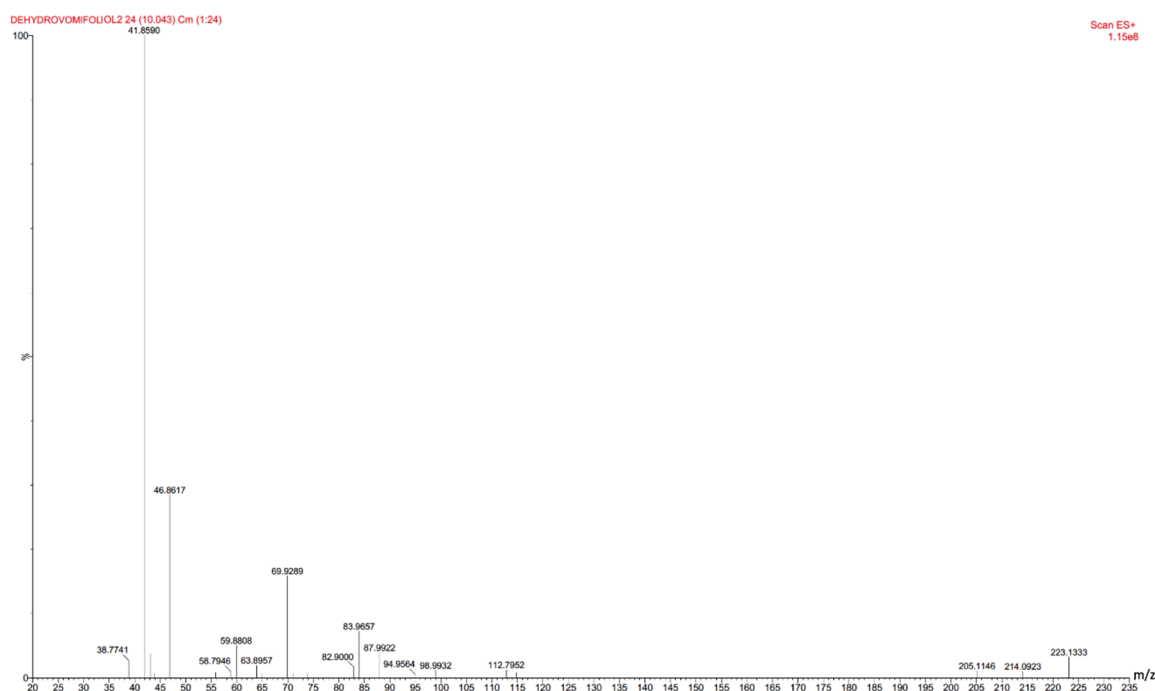
Figure 3. Mass spectrum of metabolite I obtained in the positive electrospray ionization mode. ESI–TOF MS *m/z* (relative intensity): 223.1333 ($C_{13}H_{18}O_3$, calcd 223.1334) [M + H]$^+$ (3), 205.1225 ($C_{13}H_{17}O_2$, calcd 205.1229) [M + H-H_2O]$^+$ (1), 87.9922 ($C_3H_4O_3$, calcd 88.0160) (4), 69.9989 ($C_3H_2O_2$, calcd 70.0055) (16), 46.8617 (CH_3O_2, calcd 47.0133) (28), 41.8590 (C_2H_2O, calcd 42.0106) (100).

3.4. Optical Spectroscopy

A transmission FTIR spectrum of metabolite I is shown in Figure 4.
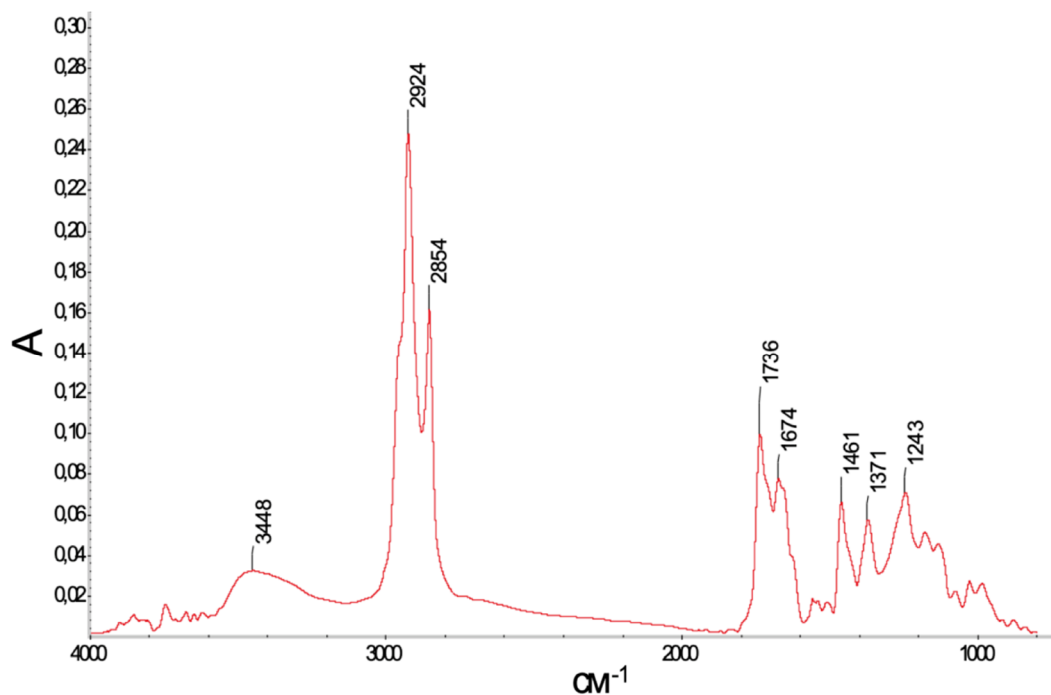
Figure 4. A transmission FTIR spectrum of metabolite I. IR (ν_{max}, cm^{-1}; band shape and vibration type assignments are given in parentheses): 3448 (broad; ν OH); 3000 (shoulder, weak; ν =C–H); 2955 (shoulder, strong), 2924, 2854 (ν_{as} CH_3, ν_{as} CH_2, ν_s CH_3, ν_s CH_2); 1736 (asymmetric, broad; ν C=O), 1674 (asymmetric, broad; ν C=C), 1461 (asymmetric; δ_{as} CH_3, scissoring δ CH_2), 1371 (δ_s CH_3), 1243 (broad; ν C–CH_3, C–C).

An UV spectrum of metabolite I was recorded in the HPLC experiment. This spectrum has one peak with an absorption maximum at 239 nm (Figure S3).

4. Discussion

The comparison of the spectra of ABA and metabolite I made it easier to identify the structure of the latter. In addition, this made it possible to clarify the spectral characteristics of ABA previously published (https://www.chemicalbook.com/CASEN_21293-29-8.htm#SpectrumDetail, accessed 12 December 2020). Basically, the spectra obtained here for ABA were identical to spectra obtained earlier, with the exception of the assignment of signals from protons 3 and 2. The assignment of the given signals to the corresponding protons made previously should be swapped, which follows from the analysis of our two-dimensional spectra. The same should be carried out with the signals from protons four and five. All chemical shifts of ^{13}C atoms in the given spectrum are by 2–3 ppm less than in the spectrum obtained in the present study. This can be explained by the difference in the anchoring of the reference peak (in our case, the $CHCl_3$ peak).

Despite the large amount of material (25 mg) taken for the ^{13}C NMR spectrum, we were unable to detect the peaks of the C-1 and C-1′ quaternary carbon atoms. The position of these atoms was established by analyzing the ^{13}C-^{1}H long-range spin-spin interactions in the HMBC spectrum.

The comparison of the NMR spectra of ABA and metabolite I showed their identity in the cyclohexenone part of the molecule, including the methyl substituents. This confirms the assumption made on the basis of mass spectrometry that the biodegradation of the ABA molecule begins from the side chain. In turn, the structure of the side chain of metabolite I can be obtained by analyzing one- and two-dimensional NMR spectra. In contrast to ABA, the double bond of the side chain of metabolite I is conjugated not with the next double bond, but with the carbonyl group, which is confirmed by the displacement of the chemical shifts of the corresponding carbon atoms toward a weaker field.

Taken together, the obtained spectral characteristics coincided with the characteristics of dehydrovomifoliol, (*4RS*)-4-hydroxy-3,5,5-trimethyl-4-[(*E*)-3-oxobut-1-enyl]cyclohex-2-en-1-one), published earlier [43,44]. The structure of this compound is shown in Figure 5.
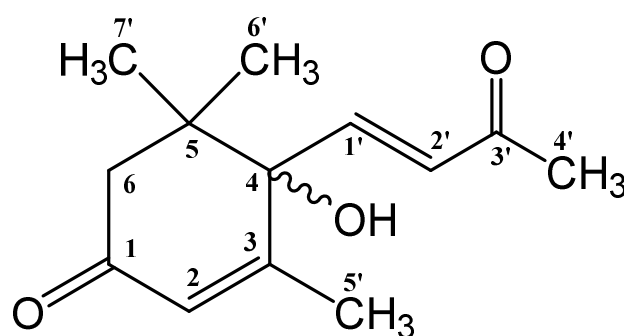

Figure 5. Structure of dehydrovomifoliol obtained from the results of the analysis of NMR and mass spectra.

The interpretation of the FTIR spectrum of the obtained metabolite I (Figure 4) deserves special attention, as it provides additional information confirming the structure of this compound. Modern FTIR spectroscopy has been increasingly applied in microbiology-related studies for both qualitative (structural) and quantitative bioanalyses (see, e.g., [45–47]). In addition, the data available on IR studies of dehydrovomifoliol cannot be considered as exhaustive. Takasugi et al. [48] indicated only four bands (by their maxima only) in a spectrum measured in $CHCl_3$. In that case, the authors of [48] did not indicate the concentration of the solvent, which makes it difficult to assess its possible role in shifting the band maxima. Häusler et al. [49] gave more spectroscopic bands (not presenting the spectrum either) measured in CCl_4. The comparison of the published infrared spectroscopic data

with those obtained in this work (for the purified substance without a solvent) shows their general similarity.

The differences in the positions of the bands are evidently caused by the influence of the solvents chosen for the measurements in [48,49]. The authors of [48,49] also did not indicate the concentrations of dehydrovomifoliol. However, taking into account the shift of the maximum of the broad stretching vibration band of the OH group (3580 cm^{-1} as indicated in [49]) to the lower frequency region (~3448 cm^{-1}; see Figure 4), it can be assumed that the intermolecular association of the OH groups in a CCl$_4$ solution [49] is insignificant as compared to that in our spectrum (where the recording conditions were in the pure condensed phase). For the C–H stretching vibrations, Häusler at al. [49] gave only one band (at 2960 cm^{-1}), which is probably due to the low resolution of their measuring equipment. However, since the dehydrovomifoliol molecule has four methyl groups and one methylene group, each of them should give two different bands of asymmetric and symmetric stretching vibrations within the region 3000–2800 cm^{-1}. In addition, there are three =CH moieties (which usually give weak FTIR stretching C–H bands near or slightly above 3000 cm^{-1}). Thus, the spectrum obtained in this work with strong and clearly asymmetric (i.e., composite) bands at 2924 and 2854 cm^{-1} is more informative reflecting the structure of the title compound.

In the spectrum of dehydrovomifoliol in the region 1600–1750 cm^{-1}, there should be at least four neighboring bands: two strong, corresponding to the different carbonyl groups (see Figure 5), and two weak, corresponding to stretching vibrations of the C=C bonds. As described earlier (Bellamy, p. 55, Table 2 [50]), conjugation of the C=C bond with the carbonyl group increases the intensity of stretching C=C vibrations. In addition, the effect of the substituent (the OH group), which is in the allyl position to both double bonds, is similar to the effect of halogens and is expected to shift the bands of stretching C=O and C=C vibrations to higher frequencies.

Indeed, in the obtained spectrum (see Figure 4), two bands of comparable intensities can be noted at 1736 and 1674 cm^{-1}. The first of them evidently corresponds to the stretching vibrations of the C=O groups, the second to the C=C bonds. Both bands exhibit asymmetry, which is explained by a superposition of two neighboring bands of structurally nonequivalent carbonyl groups and C=C moieties (see Figure 5) in each of the two bands. For the band at 1371 cm^{-1}, its δ_s assignment is typical. In Bellamy's monograph [50], it is indicated for C–CH$_3$ and C(CH$_3$)$_2$ (with the possibility of two bands) in the narrow range 1365–1385 cm^{-1}. In the spectrum obtained here, there is a band in this region with a noticeable broadening.

For the UV spectra of dehydrovomipholiol and ABA, we calculated the theoretical absorption wavelength maxima for the $\pi \to \pi^*$ transitions according to Woodward's empirical rules [51]. For a system of double bonds conjugated with a carboxyl group in ABA, this calculation leads to a value of 260 nm. In this case, the base value $\lambda_0 = 200$ nm in the calculations was taken to be the absorption maximum in the spectrum of acrylic acid (Figure 6): $\lambda_{max} = \lambda_0 + \Delta\lambda alk^\beta + \Delta\lambda alk^\delta + \Delta\lambda(C=C) = 200 + 12 + 18 + 30 = 260$ nm. This value correlates well with the experimental absorption maximum for ABA, which is in the range 263–265 nm, depending on the measuring conditions. The slight difference is possibly due to the fact that the carboxyl group is internally hydrogen bonded to the hydroxyl in the cycle.

According to the data presented above, the bacterial destruction of the ABA molecule begins from the side chain and affects one of the conjugated double bonds. This should lead to a shift in the absorption wavelength maximum of the $\pi \to \pi^*$ transition to the short-wavelength region.

For dehydrovomifoliol, the calculated value of the absorption maximum is $\lambda_{max} = \lambda_0 + 2\Delta\lambda alk^\beta = 215 + 2 \times 12 = 239$ nm, where $\lambda_0 = 215$ nm is the value indicated for cyclic enones in six-membered cycles. The obtained value coincides with the absorption wavelength of the revealed ABA metabolite and may be an indirect confirmation of the found structure.
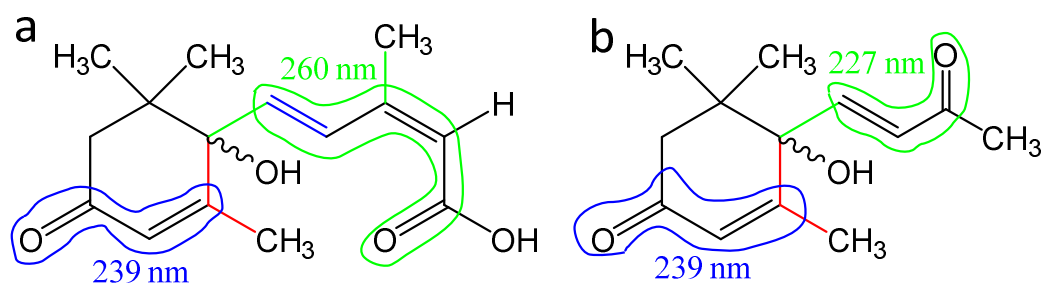
Figure 6. Systems of double bonds in ABA (**a**) and dehydrovomipholiol (**b**) which determine the base value of λ_0 for calculating the maximum UV absorption wavelength.

Until now, the role of microorganisms in maintaining ABA homeostasis in soil remains unclear. Apparently, bacteria capable of degrading ABA such as *Rhodococcus* sp. P1Y use this phytohormone as a sole source of carbon and energy [41]. The well-known pathway of ABA transformation is the modification of the cyclohexene part of the molecule with the formation of phaseic and dehydrophaseic acids, which is characteristic for plants and also proposed for soil microbial communities [6]. The report on the detection of dehydrovomifoliol as the main degradation product in the culture of soil bacterium *Corynebacterium* sp. [40] did not receive, in our opinion, due attention. In the present study, we demonstrated the ability of the rhizosphere bacterium *Rhodococcus* sp. P1Y to decompose ABA with the formation of dehydrovomifoliol when growing on an artificial nutrient medium containing this phytohormone as a sole carbon and energy source. It should be noted that the above-mentioned *Corynebacterium* sp. co-metabolized ABA in the presence of yeast extract in high concentration [40]. The presence of at least one more metabolite (metabolite II) in the culture liquid of *Rhodococcus* sp. P1Y having a lower molecular weight (Figure 1), indicates further decomposition of ABA in the course of an unknown metabolic pathway. This metabolite II is currently being studied.

There are currently no sufficient experimental data to describe a possible reaction mechanism for ABA conversion to dehydrovomifoliol. The presence of a branching point at position three of the ABA molecule may hinder normal β-oxidation. However, in the literature there are evidences for overcoming the branching point by soil bacteria. Accordingly, *Nocardia cyriacigeorgica* was able to shorten β-methylcinnamic acid due to the cleavage of the C2-unit with the formation of acetophenone [52]. As for *Rhodococcus* sp. P1Y, we can assume the elimination of the C2-unit in the reaction of meta-terminal oxidation by the mechanism proposed earlier for the degradation of alkenes by *Acinetobacter radioresistens* [53]. In this case, the second product of the ABA decomposition would be oxalic acid. However, we were unable to detect oxalic acid in the studied samples. The formation of glycolic or glyoxylic acids as a result of oxidation or acetic acid as a result of double bond cleavage can be considered as alternative options. However, our experiments with batch cultures showed that among these substrates, only acetate supported the growth of *Rhodococcus* sp. P1Y (Figure 7). Our genomic studies revealed an impressive arsenal of hydrolytic enzymes, as well as oxygenases, in ABA-utilizing bacteria *Rhodococcus* sp. P1Y [54] and *Novosphingobium* sp. P6W [55]. The precise establishment of the reaction mechanism, identification of the products of the subsequent dehydrovomifoliol degradation, and determination of the enzymes involved in these processes are now under study.

Another question that would be interesting to elucidate is the absolute configuration of the C-4 in dehydrovomifoliol formed by the bacterium. Since this would require X-ray crystallography which cannot be performed with a liquid sample, and the compound does not contain an atom with a high atomic weight, this task is quite problematic. The geometry optimization of two enantiomers, performed by us using the GAUSSIAN09 program and DFT calculations, has shown that the enantiomers have similar energies: the difference is less than 0.5 kcal/mol, which is within the limits of calculation accuracy and thus no

reliable prediction of ORD (optical rotatory dispersion) or CD (circular dichroism) spectra can be made.
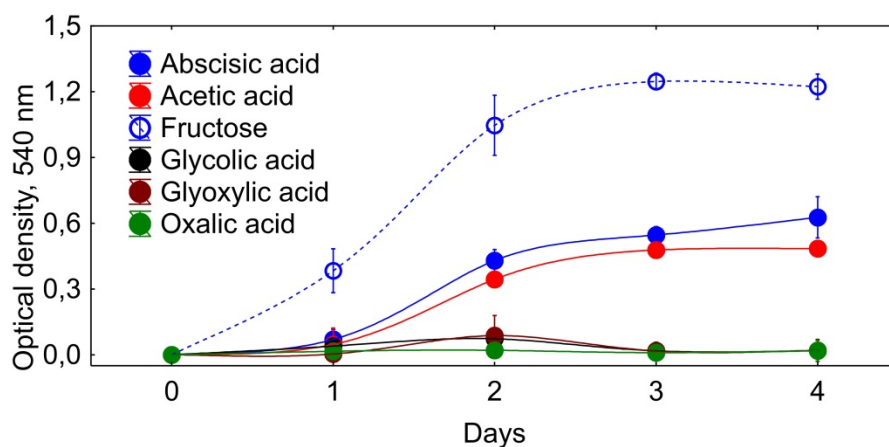

Figure 7. Growth of *Rhodococcus* sp. P1Y in a liquid mineral salt medium supplemented with different compounds as a sole carbon source. Carbon sources are shown in the figure. Vertical bars indicate confidence intervals ($n = 3$; $p < 0.05$).

5. Conclusions

During the cultivation of the rhizosphere bacterium *Rhodococcus* sp. P1Y on the medium supplemented with ABA as a sole carbon source, two metabolites of this phytohormone were detected. A detailed characterization showed that the main metabolite is dehydrovomifoliol. The results obtained allow us to conclude that there is an uncharacterized pathway of ABA degradation by rhizosphere bacteria starting with the shortening of the acyclic part of the molecule.

Conflicts of Interest: The authors declare no conflict of interest.

References

1. Zeevaart, J.A.D.; Creelman, R.A. Metabolism and Physiology of Abscisic Acid. *Annu. Rev. Plant Physiol. Plant Mol. Biol.* **1988**, *39*, 439–473. [CrossRef]
2. Nambara, E.; Marion-Poll, A. Abscisic Acid Biosynthesis and Catabolism. *Annu. Rev. Plant Biol.* **2005**, *56*, 165–185. [CrossRef] [PubMed]
3. Chen, K.; Li, G.; Bressan, R.A.; Song, C.; Zhu, J.; Zhao, Y. Abscisic acid dynamics, signaling and functions in plants. *J. Integr. Plant. Biol.* **2020**, *62*, 25–54. [CrossRef]
4. Kushiro, T.; Okamoto, M.; Nakabayashi, K.; Yamagishi, K.; Kitamura, S.; Asami, T.; Hirai, N.; Koshiba, T.; Kamiya, Y.; Nambara, E. The Arabidopsis cytochrome P450 CYP707A encodes ABA 8′-hydroxylases: Key enzymes in ABA catabolism. *EMBO J.* **2004**, *23*, 1647–1656. [CrossRef]
5. Cutler, A.J.; Krochko, J.E. Formation and breakdown of ABA. *Trends Plant Sci.* **1999**, *4*, 472–478. [CrossRef]
6. Hartung, W.; Sauter, A.; Turner, N.; Fillery, I.; Heilmeier, H. Abscisic acid in soils: What is its function and which factors and mechanisms influence its concentration? *Plant Soil* **1996**, *184*, 105–110. [CrossRef]
7. Hartung, W. The evolution of abscisic acid (ABA) and ABA function in lower plants, fungi and lichen. *Funct. Plant Biol.* **2010**, *37*, 806–812. [CrossRef]
8. Olds, C.L.; Glennon, E.K.K.; Luckhart, S. Abscisic acid: New perspectives on an ancient universal stress signaling molecule. *Microbes Infect.* **2018**, *20*, 484–492. [CrossRef] [PubMed]
9. Negri, P.; Maggi, M.D.; Ramirez, L.; De Feudis, L.; Szwarski, N.; Quintana, S.; Equaras, M.J.; Lamarttina, L. Abscisic acid enhances the immune response in *Apis mellifera* and contributes to the colony fitness. *Apidologie* **2015**, *46*, 542–557. [CrossRef]
10. Magnone, M.; Ameri, P.; Salis, A.; Andraghetti, G.; Emionite, L.; Murialdo, G.; De Flora, A.; Zocchi, E. Microgram amounts of abscisic acid in fruit extracts improve glucose tolerance and reduce insulinemia in rats and in humans. *FASEB J.* **2015**, *29*, 4783–4893. [CrossRef] [PubMed]
11. Forchetti, G.; Masciarelli, O.; Alemano, S.; Alvares, D.; Abdala, G. Endophytic bacteria in sunflower (*Helianthus annuus* L.): Isolation, characterization, and production of jasmonates and abscisic acid in culture medium. *Appl. Microbiol. Biotechnol.* **2007**, *76*, 1145–1152. [CrossRef]
12. Cohen, C.; Travaglia, N.; Bottini, R.; Piccoli, N. Participation of abscisic acid and gibberellins produced by endophytic *Azospirillum* in the alleviation of drought effects in maize. *Botany* **2009**, *87*, 455–462. [CrossRef]
13. Piccoli, P.; Lucangeli, D.; Schneider, G.; Bottini, R. Hydrolysis of [17,17-2H2] Gibberellin A20-Glucoside and [17,17-2H2] Gibberellin A20-glucosyl ester by *Azospirillum lipoferum* cultured in a nitrogen-free biotin-based chemically-defined medium. *Plant Growth Regul.* **1997**, *23*, 179–182. [CrossRef]
14. Sgroy, V.; Cassán, F.; Masciarelli, O.; Del Papa, M.; Lagares, A.; Luna, V. Isolation and characterization of endophytic plant growth-promoting (PGPB) or stress homeostasis-regulating (PSHB) bacteria associated to the halophyte *Prosopis strombulifera*. *Appl. Microbiol. Biotechnol.* **2009**, *85*, 371–381. [CrossRef] [PubMed]
15. Crocoll, C.; Kettner, J.; Dorffling, K. Abscisic acid in saprophytic and parasitic species of fungi. *Phytochemistry* **1991**, *30*, 1059–1060. [CrossRef]
16. Schmidt, K.; Pflugmacher, M.; Klages, S.; Mäser, A.; Mock, A.; Stahl, D. Accumulation of the hormone abscisic acid (ABA) at the infection site of the fungus *Cercospora beticola* supports the role of ABA as a repressor of plant defence in sugar beet. *Mol. Plant Pathol.* **2009**, *9*, 661–673. [CrossRef]
17. Spence, C.; Bias, H. Role of plant growth regulators as chemical signals in plant-microbe interactions: A double-edged sword. *Curr. Opin. Plant Biol.* **2015**, *27*, 52–58. [CrossRef]
18. Davies, W.J.; Zhang, J. Root signals and the regulation of growth and development of plants in drying soil. *Annu. Rev. Plant Physiol. Plant Mol. Biol.* **1991**, *42*, 55–76. [CrossRef]
19. Dodd, I.C.; Puértolas, J.; Huber, K.; Pérez-Pérez, J.G.; Wright, H.R.; Blackwell, M.S. The importance of soil drying and re-wetting in crop phytohormonal and nutritional responses to deficit irrigation. *J. Exp. Bot.* **2015**, *66*, 2239–2252. [CrossRef]
20. Mulkey, T.J.; Evans, M.L.; Kuzmanoff, K.M. The kinetics of abscisic acid action on root growth and gravitropism. *Planta* **1983**, *157*, 150–157. [CrossRef]
21. Pilet, P.E.; Rebeaud, J.E. Effect of abscisic acid on growth and indolyl-3- acetic acid levels in maize roots. *Plant Sci. Lett.* **1983**, *31*, 117–122. [CrossRef]

22. Sharp, R.E.; LeNoble, M.E. ABA, ethylene and the control of shoot and root growth under water stress. *J. Exp. Bot.* **2002**, *53*, 33–37. [CrossRef] [PubMed]

23. Kutschera, U.; Schopfer, P. Effect of auxin and abscisic acid on cell wall extensibility in maize coleoptiles. *Planta* **1986**, *167*, 527–535. [CrossRef]

24. Gaciarrubio, A.; Legaria, J.P.; Covarrubias, A.A. Abscisic acid inhibits germination of mature Arabidopsis seeds by limiting the availability of energy and nutrients. *Planta* **1997**, *203*, 182–187. [CrossRef] [PubMed]

25. Henfling, J.W.D.M.; Bostock, R.; Kuc, J. Effect of abscisic acid on rishtin and lubimin accumulation and resistance *to Phytophtora binfestans* and *Cladosporium cucumerinum* in potato tuber tissue slices. *Phytopathology* **1980**, *70*, 1074–1078. [CrossRef]

26. Mohr, P.G.; Cahill, D.M. Abscisic acid influences the susceptibility of Arabidopsis thaliana to Pseudomonas syringae pv. tomato and Peronospora parasitica. *Funct. Plant Biol.* **2003**, *30*, 461–469. [CrossRef]

27. Ward, E.W.B.; Cahill, D.M.; Bhattacharyya, M.K. Abscisic acid suppression of phenylalanine ammonia-lyase activity and mRNA and resistance of soybeans to *Phytophthora megasperma* f.sp. glycinea. *Plant Physiol.* **1989**, *91*, 23–27. [CrossRef]

28. Asselbergh, B.; Achuo, A.E.; Höfte, M.; Van Gijsegem, F. Abscisic acid deficiency leads to rapid activation of tomato defence responses upon infection with Erwinia chrysanthemi. *Mol. Plant Pathol.* **2008**, *9*, 11–24. [CrossRef]

29. Dodd, I.; Zinovkina, N.; Safronova, V.; Belimov, A. Rhizobacterial mediation of plant hormone status. *Ann. Appl. Biol.* **2010**, *157*, 361–379. [CrossRef]

30. Belimov, A.A.; Dodd, I.C.; Safronova, V.I.; Shaposhnikov, A.I.; Azarova, T.S.; Makarova, N.M.; Davies, W.J.; Tikhonovich, I.A. Rhizobacteria that produce auxins and contain ACC deaminase decrease amino acid concentrations in the rhizosphere and improve growth and yield of well-watered and water-limited potato (*Solanum tuberosum*). *Ann. Appl. Biol.* **2015**, *167*, 11–25. [CrossRef]

31. Zúñiga, A.; Poupin, M.J.; Donoso, R.; Ledger, T.; Guiliani, N.; Gutiérrez, R.A.; González, B. Quorum Sensing and Indole-3-Acetic Acid Degradation Play a Role in Colonization and Plant Growth Promotion of Arabidopsis thaliana by Burkholderia phytofirmans PsJN. *Mol. Plant. Microbe Interact.* **2013**, *26*, 546–553. [CrossRef]

32. Leveau, J.H.J.; Gerards, S. Discovery of a bacterial gene cluster for catabolism of the plant hormone indole 3-acetic acid. *FEMS Microbiol. Ecol.* **2008**, *65*, 238–250. [CrossRef]

33. Olesen, M.R.; Jochimsen, B.U. Identification of enzymes involved in indole-3-acetic acid degradation. *Plant Soil* **1996**, *186*, 143–149. [CrossRef]

34. Taylor, J.; Zaharia, L.; Chen, H.; Anderson, E.; Abrams, S. Biotransformation of adenine and cytokinins by the rhizobacterium *Serratia proteamaculans*. *Phytochemistry* **2006**, *67*, 1887–1894. [CrossRef]

35. Cassán, F.; Bottini, R.; Schneider, G.; Piccoli, P. *Azospirillum brasilense* and *Azospirillum lipoferum* hydrolyze conjugates of GA_{20} and metabolize the resultant aglycones to GA_1 in seedlings of rice dwarf mutants. *Plant Physiol.* **2001**, *125*, 2053–2058. [CrossRef] [PubMed]

36. Yen, K.M.; Serdar, C.M. Genetics of naphthalene catabolism in pseudomonads. *Crit. Rev. Microbiol.* **1988**, *15*, 247–268. [CrossRef] [PubMed]

37. Sazonova, O.I.; Izmalkova, T.Y.; Kosheleva, I.A.; Boronin, A.M. Salicylate degradation by *Pseudomonas putida* strains not involving the "Classical" *nah2* operon. *Microbiology* **2008**, *77*, 710–716. [CrossRef]

38. Nascimento, F.X.; Glick, B.R.; Rossi, M.J. Isolation and characterization of novel soil- and plant-associated bacteria with multiple phytohormone-degrading activities using a targeted methodology. *Access Microbiol.* **2019**, *1*, e000053. [CrossRef]

39. Lievens, L.; Pollier, J.; Goossens, A.; Beyaert, R.; Staal, J. Abscisic Acid as Pathogen Effector and Immune Regulator. *Front. Plant Sci.* **2017**, *8*, 587. [CrossRef]

40. Hasegawa, S.; Poling, S.; Mayer, V.; Bennett, R. Metabolism of abscisic acid: Bacterial conversion to dehydrovomifoliol and vomifoliol dehydrogenase activity. *Phytochemistry* **1984**, *23*, 2769–2771. [CrossRef]

41. Belimov, A.A.; Dodd, I.C.; Safronova, V.I.; Dumova, V.A.; Shaposhnikov, A.I.; Ladatko, A.G.; Davies, W.J. Abscisic acid metabolizing rhizobacteria decrease ABA concentrations in planta and alter plant growth. *Plant Physiol. Biochem.* **2014**, *7*, 84–91. [CrossRef]

42. Shevchenko, V.P.; Nagaev, I.Y.; Shaposhnikov, A.I.; Shevchenko, K.V.; Belimov, A.A.; Batasheva, S.N.; Gogoleva, N.E.; Myasoedov, N.F. Synthesis and Testing of Abscisic Acid with Predominant Replacement of Protium Atoms by Tritium in the Cyclohexene Moiety. *Dokl. Chem.* **2018**, *483*, 268–271. [CrossRef]

43. Zaman, F.; Iwasaki, A.; Suenaga, K.; Kato-Noguchi, H. Two allelopathic substances from *Paspalum commersonii* Lam. *Acta Agric. Scand. Soil Plant Sci.* **2018**, *68*, 342–348.

44. Schievano, E.; Morelato, E.; Facchin, C.; Mammi, C. Characterization of Markers of Botanical Origin and Other Compounds Extracted from Unifloral Honeys. *J. Agric. Food Chem.* **2013**, *61*, 1747–1755. [CrossRef] [PubMed]

45. Lasch, P.; Naumann, D. Infrared spectroscopy in microbiology. In *Encyclopedia of Analytical Chemistry*; Meyers, R.A., Ed.; John Wiley & Sons: Hoboken, NJ, USA, 2015. [CrossRef]

46. Kamnev, A.A.; Tugarova, A.V.; Dyatlova, Y.A.; Tarantilis, P.A.; Grigoryeva, O.P.; Fainleib, A.M.; De Luca, S. Methodological effects in Fourier transform infrared (FTIR) spectroscopy: Implications for structural analyses of biomacromolecular samples. *Spectrochim. Acta Part A Mol. Biomol. Spectrosc.* **2018**, *193*, 558–564. [CrossRef] [PubMed]

47.	Tugarova, A.V.; Dyatlova, Y.A.; Kenzhegulov, O.A.; Kamnev, A.A. Poly-3-hydroxybutyrate synthesis by different *Azospirillum brasilense* strains under varying nitrogen deficiency: A comparative *in-situ* FTIR spectroscopic analysis. *Spectrochim. Acta Part A Mol. Biomol. Spectrosc.* **2021**, *252*, 119458. [CrossRef]

48.	Takasugi, M.; Anetai, M.; Katsui, N.; Masamune, T. The occurrence of vomifoliol, dehydrovomifoliol and dehydrophaseic acid in the roots of "kidney bean" (*Phaseolus vulgaris* L.). *Chem. Lett.* **1973**, *2*, 245–248. [CrossRef]

49.	Häusler, M.; Montag, A. Isolation, identification and quantitative determination of the norisoprenoid (*S*)-(+)-dehydrovomifoliol in honey. *Z. Lebensm. Unters. Forsch.* **1989**, *189*, 113–115. [CrossRef]

50.	Bellamy, L.J. *The Infra-Red Spectra of Complex Molecules*; John Wiley & Sons: Hoboken, NJ, USA, 1957.

51.	Brown, D.W.; Floyd, A.J.; Sainsbury, M. *Organic Spectroscopy*; Wiley: Chichester, UK, 1988; 258p.

52.	Nhi-Cong, L.T.; Mikolasch, A.; Awe, S.; Sheikhany, H.; Klenk, H.-P.; Schauer, F. Oxidation of aliphatic, branched chain, and aromatic hydrocarbons by *Nocardia cyriacigeorgica* isolated from oil-polluted sand samples collected in the Saudi Arabian Desert. *J. Basic Microbiol.* **2010**, *50*, 241–253. [CrossRef] [PubMed]

53.	Minerdi, D.; Zgrablic, I.; Sadeghi, S.J.; Gilardi, G. Identification of a novel Baeyer-Villiger monooxygenase fromAcinetobacter radioresistens: Close relationship to the *Mycobacterium tuberculosis* prodrug activator EtaA. *Microb. Biotechnol.* **2012**, *5*, 700–716. [CrossRef]

54.	Gogoleva, N.E.; Nikolaichik, Y.A.; Ismailov, T.T.; Khlopko, Y.A.; Dmitrieva, S.A.; Konnova, T.A.; Ermekkaliev, T.S.; Safronova, V.I.; Belimov, A.A.; Gogolev, Y.V. Complete Genome Sequence of Abscisic Acid-Metabolizing Rhizobacterium *Rhodococcus* sp. Strain P1Y. *Microbiol. Resour. Announc.* **2019**, *8*, e01591-18. [CrossRef] [PubMed]

55.	Gogoleva, N.E.; Nikolaichik, Y.A.; Ismailov, T.T.; Khlopko, Y.A.; Dmitrieva, S.A.; Konnova, T.A.; Ermekkaliev, T.S.; Safronova, V.I.; Belimov, A.A.; Gogolev, Y.V. Complete genome sequence of the abscisic acid-utilizing strain *Novosphingobium* sp. P6W. *3 Biotech* **2019**, *9*, 94. [CrossRef] [PubMed]